



Synthesis, experimental and theoretical study of novel 2-haloalkyl (-CF₂H, -CCl₂H, -CF₂CF₃)-, 3-bromo and bromomethyl substituted chromones

Ena G. Narváez O^a, Pablo M. Bonilla V.^a, Daniel A. Zurita^a, Christian D. Alcívar L.^{a,b,*}, Jorge Heredia-Moya^{c,**}, Sonia E. Ulic^{d,e}, Jorge L. Jios^{f,g}, Oscar E. Piro^h, Gustavo A. Echeverría^h, Peter Langer^{i,j}

^a Facultad de Ciencias Químicas, Universidad Central del Ecuador, Francisco Viteri s/n y Gilberto Gato Sobral, Quito, Ecuador

^b Centro de Investigación de Alimentos, CIAL, Facultad de Ciencias de la Ingeniería e Industrias, Universidad UTE, EC171029, Quito, Ecuador

^c Centro de Investigación Biomédica (CENBIO), Facultad de Ciencias de la Salud Eugenio Espejo, Universidad UTE, 170147, Quito, Ecuador

^d CEQUINOR (CONICET-UNLP), Facultad de Ciencias Exactas, Universidad Nacional de La Plata, 47 esq. 115, 1900, La Plata, Argentina

^e Departamento de Ciencias Básicas, Universidad Nacional de Luján, Rutas 5 y 7, 6700, Luján, Buenos Aires, Argentina

^f Laboratorio UPL (UNLP-CIC), Campus Tecnológico Gonnet (CIC-BA), Cno. Centenario e/505 y 508, 1897, Gonnet, Argentina

^g Departamento de Química, Facultad de Ciencias Exactas, Universidad Nacional de La Plata, 47 esq. 115, 1900, La Plata, Argentina

^h Departamento de Física, Facultad de Ciencias Exactas, Universidad Nacional de La Plata e IFLP (CONICET, CCT-La Plata), C.C. 67, 1900, La Plata, Argentina

ⁱ Institut für Chemie, Universität Rostock, Albert-Einstein-Str. 3a, 18059, Rostock, Germany

^j Leibniz Institut für Katalyse, Universität Rostock e. V. (LIKAT), Albert-Einstein-Str. 29a, 18059, Rostock, Germany

ARTICLE INFO

Keywords:

2-haloalkyl chromones
Spectroscopic properties
Structural X-ray diffraction
Quantum chemical calculations
Hirshfeld surface analysis
Halogen bonds

ABSTRACT

A set of seven new chromones with 2-haloalkyl (-CF₂H, -CCl₂H, -CF₂CF₃) and 3-bromo and bromomethyl substituents were synthesized. The novel compounds were studied by DFT calculations and characterized by vibrational spectroscopy (IR and Raman) in solid state, and NMR (¹H, ¹³C and ¹⁹F) and UV-vis spectroscopy in solution. The crystal structure of 3-dibromomethyl-2-difluoromethyl chromone was determined by X-ray diffraction. Due to extended π-bond delocalization, the organic framework is planar and lies on a crystallographic m-mirror plane. The intermolecular non-covalent interactions of 3-dibromomethyl-2-difluoromethyl chromone, as π...π stacking arrangements, F...H hydrogen bonds and O...Br contacts were evaluated by Hirshfeld surfaces analysis. These intermolecular contacts, which affect the absorption bands location of the involved groups, were also detected in the vibrational spectra.

1. Introduction

The role of non-covalent interactions in small molecules has special attraction in the develop of new materials[1,2], sensors[3,4], bioactive compounds[5] and their descriptions of host-guest interactions[6]. Non-covalent interactions of weak to medium intensity are observed between halogen containing molecules and lone pairs of a Lewis base or π electrons of unsaturated systems generally[7], these interactions are often referred to as halogen bonding. Moreover, crystallographic studies show halogen bonds in biological systems responsible of molecular recognition like thyroid hormone[8], small molecule-protein complexes [9] like anesthetics-ferritin, Diclofenac-COX-2, Triclosan-enoyl-acyl carrier protein reductase.

On the other hand, chromones are an important class of oxygen-containing heterocyclic compounds[10,11] and exhibit interesting and diverse biological activities[12,13]. In fact, recent reviews highlight the role of chromones in medicinal chemistry[14] as a privileged scaffold in drug discovery[13,15,16]. Therefore, research related to synthesis and transformation of chromone derivatives has increased in recent years [17,18], where halogen-containing chromones show enhanced biological activities[19]. In this sense, it is well known that the introduction of halogen atoms in compounds with potential biological activity improve their pharmacokinetic and lipophilicity properties[20,21]. Accordingly, some halo-substituted chromone derivatives show better action as antitumor[22–24], cardioprotective[25] and antimicrobial agents[13, 26,27]. Besides, these compounds have importance as synthetic building

* Corresponding author at: Facultad de Ciencias Químicas, Universidad Central del Ecuador, Francisco Viteri s/n y Gilberto Gato Sobral, Quito, Ecuador.

** Corresponding author.

E-mail addresses: cdalcivar@uce.edu.ec (C.D. Alcívar L.), jorgeh.heredia@ute.edu.ec (J. Heredia-Moya).

<https://doi.org/10.1016/j.jfluchem.2020.109717>

Received 10 August 2020; Received in revised form 15 December 2020; Accepted 17 December 2020

Available online 4 January 2021

0022-1139/© 2020 Elsevier B.V. All rights reserved.

blocks, due to their high reactivity[12,25,28], and are often used in organic synthesis to form new heterocycles[29–31]. The versatility of such halogenated heterocycles, as intermediates, is an interesting feature that can be employed to access new methyl chromone derivatives using simple nucleophiles[5].

The novel chromones **1**–**7** were synthesized by a standard two-step procedure involving a one-pot protocol[32] using the appropriate *o*-acylphenol and haloalkyl (-CF₃, CF₂H, CCl₂H and -CF₂CF₃) anhydrides (Scheme 1). The new 3-substituted compounds with bromomethyl, dibromomethyl and bromine moieties were obtained after substitution reactions[33,34]. Although halogen-containing chromones are known since 1977[12], these compounds are privileged scaffolds[19,28] for derivatives with improved biological activities[13].

2. Results and discussion

2.1. IR and Raman spectroscopy

IR (**1**–**7**) and Raman (**1**–**4**, **6**, **7**) most representative bands are described in Table 1. The tentative assignment was assisted using theoretical calculations for the most stable conformers. Moreover, the IR and Raman spectra of solid for all compounds are shown in the Fig. S1–S2 (a–b) of the ESI.

The vibrational spectra of **1**–**7** show strong absorption bands at: 1657, 1657, 1649, 1649, 1650, 1647 and 1657 cm⁻¹ (Raman. 1652, 1663, 1669, 1642, 1704, 1644 and 1645 cm⁻¹), respectively, attributed to C=O stretching modes of the chromone ring[33,35,36]. The shifting of the C=O band, towards lower frequencies in the IR spectra, could be explained by short intermolecular contacts C_{sp2}-O...Br-C_{sp3}.

The absorptions between 1637 and 1606 cm⁻¹ are assigned to the C=C stretching for **1**–**7** and C_(sp3)-Br substitution in compounds **2**–**7** has been confirmed by weak absorption bands in the region of 633 to 587 cm⁻¹. The -CF₃ group in **1**–**3** shows very strong bands at 1154, 1177, 1173 cm⁻¹ and 1134, 1157, 1149 cm⁻¹ attributed to asymmetric C-F stretching modes, respectively. Moreover, the strong absorption bands

at 1008, 1123, 1033 cm⁻¹ were assigned to symmetric C-F stretching mode. Moreover, the compound **7**, with the CF₃CF₂- substituent, shows strong absorption bands at 1217 and 1174 cm⁻¹ (Raman. 1218 and 1176 cm⁻¹) assigned to CF₃ asymmetric stretching modes and a medium absorption band at 1130 cm⁻¹ (Raman. 1132 cm⁻¹) attributed to the CF₃ symmetric stretching mode. The band at 737 cm⁻¹ (Raman. 745 cm⁻¹) is attributed to the CF₃ deformation mode. The CF₂ symmetric and asymmetric stretching modes for compounds **4** and **5** were observed as strong absorptions at 1108 and 1118 cm⁻¹ for **4**, and at 1056 and 1068 cm⁻¹ for **5**, respectively. Likewise, the -CBr₂H group for **5** and **6** showed weak absorption bands at 646 and 642 cm⁻¹ assigned to the asymmetric stretchings, and the symmetric ones were observed at 600 and 587 cm⁻¹, respectively. In **6**, the C-Cl₂ symmetric stretching is located at 761 cm⁻¹ (Raman. 758 cm⁻¹), while its asymmetric counterpart was not observed neither in IR nor in Raman.

2.2. Electronic spectra

The calculated and experimental electronic spectra of **1**–**7**, using methanol as solvent (**1**: 4.76 × 10⁻⁶ M, **2**: 6.2 × 10⁻⁶ M, **3**: 6.2 × 10⁻⁶ M, **4**: 2.0 × 10⁻⁵ M, **5**: 3.2 × 10⁻⁵ M, **6**: 2.0 × 10⁻⁵ M, **7**: 2.0 × 10⁻⁶ M), are shown in Fig. S10. The theoretical spectra were calculated at the B3LYP/6-311++G(d,p) level of theory, considering the implicit influence of the solvent (methanol, ε = 32.7), with the conductor-like polarizable continuum model (CPCM). The molecular orbitals involved in the electronic transitions of **1**–**7** are shown in Fig. S13. Table 2 summarizes the main experimental absorption bands, which are correlated with the vertical electronic transitions with dominant oscillator strengths (f > 0.075) to support the tentative assignment.

The electronic transitions of the absorptions at 202 nm involve HOMO→LUMO + 2 for **3**, and HOMO→LUMO + 3, excitations for **5** and **6**. These bands arise from π orbitals of the aromatic ring and C2 = C3 bond, and non-bonding orbitals of oxygen, chlorine and bromine atoms to π* orbitals of the aromatic ring. This tentative assignment is in agreement with related compounds[35].

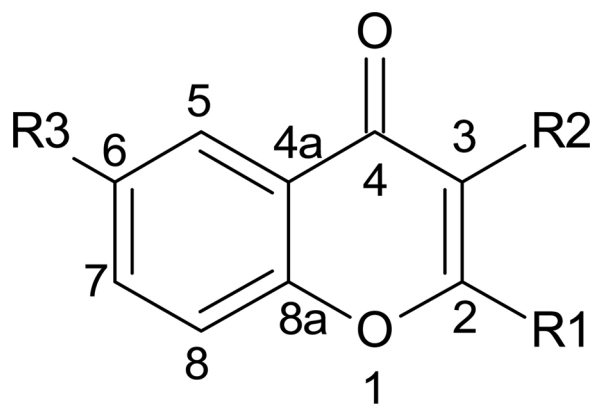
Likewise, the band at 205 nm is originated by the contribution of HOMO-2→LUMO + 1 (**1**), HOMO-2→LUMO + 3 (**2**), HOMO-5→LUMO + 1 (**4**) HOMO→LUMO + 2 (**7**) excitations. Particularly, for **1**, **4** and **5** they can be assigned to excitations from π orbitals of the chromone ring and C=C bond, and non-bonding orbitals of chlorine and bromine atoms to π* orbitals of the whole molecule. For **2**, this absorption is substantially dominated by transitions from non-bonding orbitals of the carbonyl oxygen atom and C3-C4 and C4-C5 σ orbitals to σ* orbital of the C3-Br bond.

Moreover, in the electronic spectra of **1**–**7** was observed a broad band at 319, 309, 318, 303, 340, 306, 306 nm, respectively, assigned to a sole dominant one electron excitations from HOMO to LUMO orbitals. They are basically originated by π → π* transitions throughout the molecule [5] and, particularly for **1**–**3**, also n → π*-transitions from non-bonding orbitals of chlorine and bromine atoms are involved.

The theoretical calculations suggest a significant contribution of HOMO → LUMO transitions, for the absorption bands around 300 nm of the UV-vis spectra of **1**–**7** (Table 2). The ΔE HOMO-LUMO calculated show a minor energy gap for **2** with 4.35 eV, while **4** present 4.67 eV. In this sense, the observed tendency in the HOMO/LUMO gaps show the following order **4** > **5** > **7** > **1** > **6** > **3** > **2**. This result suggests an effect of stabilization of the bromine and chlorine atoms at C-6 and C-3 in the energy HOMO/LUMO gaps for **1**–**3**, while that the electron-withdrawing effect of the CF₃, CF₂H, CCl₂H, CF₂CF₃ and CH₂Br, CHBr₂ groups at C-2 and C-3 respectively, in **4**–**7** generate upper energy HOMO/LUMO gaps, similar to observed in 2-(haloalkyl)-3-methylchromones[34,35].

2.3. Crystallographic structural results of **5**

Suitable crystals for X-ray diffraction analysis were obtained from slow and controlled solvent evaporation from a dissolution of **5** in



Comp.	R1	R2	R3
1	CF ₃	CH ₃	Cl
2	CF ₃	Br	Br
3	CF ₃	CH ₂ Br	Cl
4	CF ₂ H	CH ₂ Br	H
5	CF ₂ H	CHBr ₂	H
6	CCl ₂ H	CHBr ₂	H
7	CF ₂ CF ₃	CH ₂ Br	H

Scheme 1. New 2-haloalkyl (-CF₂H, -CCl₂H, -CF₂CF₃)-, 3-bromo and bromo-methyl substituted chromones.

Table 1Experimental and calculated frequencies (cm^{-1}) and tentative assignment of the most relevant vibrational modes for 1 – 7.

Compound 1.				
Exp. ^[a]		Calc. ^[b]		Assig. ^[f]
IR ^[c]	Raman	Freq. ^[d]	Int. ^[e]	
3083 (w)	3014 (6)	3164	6	ν_{as} (CH_3)
3055(vw)	2972(7)	3095	5	ν_{as} (CH_3)
2944(vw)	2944(9)	3049	6	ν_{s} (CH_3)
1657 (vs)	1652 (100)	1710	299	ν (C = O)
1608 (w)	1643 (36)	1671	34	ν (C = C)
1154 (vs)	1147 (8)	1165	287	ν_{as} (CF_3)
1134 (m)	1106(4)	1124	275	ν_{as} (CF_3)
1008 (w)	1001(2)	1012	49	ν_{s} (CF_3)
677 (w)	—	682	14	ν (C6-Cl)
Compound 2.				
Exp.		Calc.		Assig.
IR	Raman	Freq.	Int.	
3099 (w)	3076 (2)	3213	6	ν_{s} (C-H) ring
1657 (vs)	1663 (100)	1729	238	ν (C = O)
1613 (m)	1613 (39)	1638	49	ν (C = C)
1177(vs)	—	1189	211	ν_{as} (CF_3)
1157(vs)	—	1167	237	ν_{as} (CF_3)
1123 (s)	1125 (8)	1147	272	ν_{s} (CF_3)
725 (w)	727 (43)	723	25	δ (CF_3)
663 (w)	665 (3)	668	36	ν (C6-Br) ring
607(vw)	—	608	12	ν (C3-Br)
Compound 3.				
Exp.		Calc.		Assig.
IR	Raman	Freq.	Int.	
3097 (w)	3101 (8)	3224	3	ν_{s} (CH_2)
1649 (vs)	1669 (100)	1718	265	ν (C = O)
1606 (m)	1636 (72)	1662	84	ν (C = C)
1173(m)	1174(10)	1186	268	ν_{as} (CF_3)
1149 (vs)	1098 (4)	1131	221	ν_{as} (CF_3)
1033(m)	1011(6)	1011	51	ν_{s} (CF_3)
680(w)	680 (7)	680	20	ν (C6-Cl)
633(w)	619 (4)	607	27	ν (C3'-Br)
Compound 4.				
Exp.		Calc.		Assig.
IR	Raman	Freq.	Int.	
2925 (vw)	3003 (10)	3137	15	ν (CF_2 -H)
2853 (vw)	2997 (9)	3121	7	ν (CH_2)
1649 (vs)	1641 (100)	1711	713	ν (C = O)
1609 (m)	1612 (11)	1668	95	ν (C = C)
1108 (s)	1109 (4)	1116	146	ν_{s} (CF_2)
1055 (vs)	1056 (3)	1047	115	ν_{as} (CF_2)
610 (w)	610 (74)	597	97	ν (C3'-Br)
559 (vw)	560 (17)	559	4	δ (CF_2)
Compound 5.				
Exp.		Calc.		Assig.
IR	Raman	Freq.	Int.	
3010 (w)	—	3180	24	ν (CBr ₂ -H)
2922 (vw)	—	3159	7	ν (CF_2 -H)
1650 (vs)	—	1704	304	ν (C = O)
1637 ^{sh} (m)	—	1665	116	ν (C = C)
1118 (s)	—	1118	187	ν_{s} (CF_2)
1068 (vs)	—	1053	180	ν_{as} (CF_2)
646 (m)	—	625	63	ν_{as} (CBr ₂)
600 (w)	—	597	35	ν_{s} (CBr ₂)
—	—	—	—	—
Compound 6.				
Exp.		Calc.		Assig.
IR	Raman	Freq.	Int.	
3028 (vw)	3060 (8)	3196	4	ν (CCl ₂ -H)
2921 (w)	3022 (4)	3181	24	ν (CBr ₂ -H)
1647 (vs)	1644 (70)	1702	310	ν (C = O)

(continued on next page)

Table 1 (continued)

Compound 6.					
Exp.		Calc.		Assig.	
IR	Raman	Freq.	Int.		
1625 (m)	1626 (48)	1654	142	ν (C = C)	
761 (s)	758 (25)	758	97	ν_s (CCL2)	
—	—	756	56	ν_{as} (CCL2)	
642 (vw)	641 (32)	622	27	ν_{as} (CBr2)	
587 (w)	590 (53)	589	44	ν_s (CBr2)	
—	349 (46)	344	56	δ (CCL2)	
Compound 7.					
Exp.		Calc.		Assig.	
IR	Raman	Freq.	Int.		
2852 (vw)	3014 (13)	3138	3	ν_s (CH ₂)	
1657 (vs)	1645 (100)	1717	279	ν (C = O)	
1630 ^{sh} (m)	1626 (69)	1657	124	ν (C = C)	
1330 (m)	1332 (20)	1296	150	ν_s (C2'-C2''), ν_s (CF ₃)	
1217 (vs)	1218 (24)	1198	243	ν_{as} (CF ₃)	
1204 (vs)	—	1194	186	ν (C-O), δ (C3-C3')	
1174 (m)	1176 (10)	1180	129	ν_{as} (CF ₃)	
1164 (m)	1165 ^{sh} (7)	1158	82	ν_{as} (CF ₂)	
1130 (m)	1132 (2)	1138	167	ν_s (CF ₃)	
737 (m)	745 (30)	737	30	δ (CF ₃)	
607 (vw)	589 (72)	601	12	ν (C3'-Br)	

[a]: Experimental. [b]: Calculated. [c]: Infrared. [d]: Frequency. [e]: Intensity. [f]: Assignment.

hexane. Fig. 1 is an ORTEP[35] drawing of **5**. The crystal data, structure refinement results, bond lengths and angles are in Table S2-S7, ESI. The substance crystallizes in the orthorhombic space group Pnma with $a = 19.772(1)$ Å, $b = 6.9580(4)$ Å, $c = 8.6313(6)$ Å, and $Z = 4$ molecules per unit cell. The structure was solved from 968 reflections with $I > 2\sigma(I)$ and refined by full-matrix least-squares to a R1-value of 0.0485. Due to extended π -bonding the chromone molecular skeleton is planar; it is sited onto a crystallographic mirror plane. Observed bond distances and angles agree with established Organic Chemistry rules. In fact, phenyl ring C—C distances [from 1.352(9) to 1.401(8) Å] are as expected for a resonant-bond structure. The fused hetero-cycle shows a C2—C3 bond length of 1.319(8) Å, shorter than the other heterocycle C—C distances [1.479(8) and 1.481(7) Å], corresponds to a formally double bond character for that link. C—O single bond distances are 1.356(8) Å and 1.387(7) Å, and carbonyl C=O double bond length is equal to 1.215(6) Å. The molecular metrics of the chromone skeleton agrees with the corresponding one of other closely related chromone derivatives [33, 36]. The $-\text{C}(\text{sp}^3)\text{F}_2\text{H}$ and $-\text{C}(\text{sp}^3)\text{Br}_2\text{H}$ groups exhibit the expected tetrahedral bonding structure with C—CF and CC—Br angles of 109.0 (5)° and 114.6(2)°, respectively, and F—C—F and Br—C—Br angles of 106.2 (7)° and 109.7(3)°. Observed C—F and C—Br bond distances are 1.337 (6) Å and 1.933(3) Å.

Fig. 2 shows a special type of intermolecular contact between bromine (of the CHBr_2 moiety) and the carbonyl oxygen atom, described by $R_4^4(14)$ second level graph set along the c axis[37]. This non-covalent interaction could be classified as type I halogen bonding[37,38], mainly due the directionality between bromine and oxygen atom, ($\angle \text{C—Br}\cdots\text{O}1 = 60.9^\circ$). The interatomic $d(\text{O}\cdots\text{Br})$ distance (3.041 Å) is minor than the sum of van der Waals radii (3.37 Å) and considerably shorter than that observed in related molecules[33] (Table 3)[39–41]. The same geometrical features are observed in 4-halotriaroylbenzenes [42]. The crystal packing also displays interhalogen $\text{Br}\cdots\text{Br}$ contacts, with a distance slightly higher (3.7978(3) Å) than that observed in 2-chlorodifluoromethyl-3-bromomethylchromone (3.621(2) Å)[33].

Moreover, the graphical representation of the energy frameworks of **5** (Table 3) is useful to evidence the interactions between molecular pairs and show the magnitude of the interaction energy displayed for E_{ele} (red cylinders), E_{dis} (green) and E_{tot} (blue). The quantification of the energy frameworks quantification was performed with CrystalExplorer 17.5[43] program, using the HF/3-21 G approximation. To visualize the

supramolecular architecture the cluster of molecules within a radius of 3.8 Å from the central molecule was considered. The results show that the $\text{C}_{\text{sp}^3}\text{—Br}\cdots\text{O—C}_{\text{sp}^2}$, $\text{C}_{\text{sp}^3}\text{—F}\cdots\text{H—C}_{\text{sp}^2}$, $\pi\cdots\pi$ and $\text{C}_{\text{sp}^3}\text{—Br}\cdots\text{Br—C}_{\text{sp}^3}$ interactions are the intermolecular contacts with the greater contribution of dispersive energy (-16.1 kJ mol⁻¹, -9.1 kJ mol⁻¹, -59.7 kJ mol⁻¹ and -7.8 kJ mol⁻¹, respectively). The energy frameworks plotted at the top of Table 3, illustrate the predominantly dispersive nature of these interactions with vertical cylinders (green) in the crystal structure. The nature of $\text{Br}\cdots\text{O}$ halogen bond was studied in di-nuclear vanadium(V) complexes with Schiff base ligands and showed the existence of a σ -hole around Br atom [44]. Except for $\pi\cdots\pi$ stacking interactions, the $\text{F}\cdots\text{H}$ are within the most effective contacts and at the same time with the lowest repulsive energy ($+1.8$ kJ mol⁻¹, Table 3), indicating that the contribution of fluorine atoms to the stabilization of the crystal lattice is of particular interest and deserves further attention.

Fig. 3 and Table 4 show the $\pi\cdots\pi$ stacking arrangement and its geometrical parameters, respectively. The 4-pyrene and benzene participate in an intermolecular network, where the rings display an offset facial arrangement, as observed in other chromones [5]. The $\pi\cdots\pi$ contacts were found to play an important role in driving layered supramolecular assembly in chromone derivatives[45].

2.4. Hirshfeld surface analysis

The Hirshfeld surface analysis was performed to understand the role of intermolecular contacts in the crystal structure of **5**. Crystal data show that the interatomic $\text{O}\cdots\text{Br}$ distance in **5** is considerably shorter than that observed in related molecules[42]. This contact could be considered as a weak non-covalent interaction, with predominant repulsive energy contribution (20.4 kJ mol⁻¹) in the crystalline lattice (see ESI, Table S8) and is showed as red spots in the d_{norm} Hirshfeld Surface (HS) (Fig. 4a). The shape index (Fig. 4b) shows adjacent red and blue triangles located at the benzene and 4-pyrene rings, and the flat regions delineated by blue outline in curvedness surface (Fig. 4c) evidence $\pi\cdots\pi$ stacking arrangements. The crystal lattice energy analysis, applying the CE-B3LYP/6-311 G(d,p) energy model, showed 3D energy frameworks of -38.6 kJ mol⁻¹ total energy (see Fig. S14), with dispersive nature $\pi\cdots\pi$ contacts (-59.7 kJ mol⁻¹) and minor contribution of repulsive energy (42.9 kJ mol⁻¹).

The 2D-fingerprint plot of **5** is displayed in Fig. 5. The label III shows

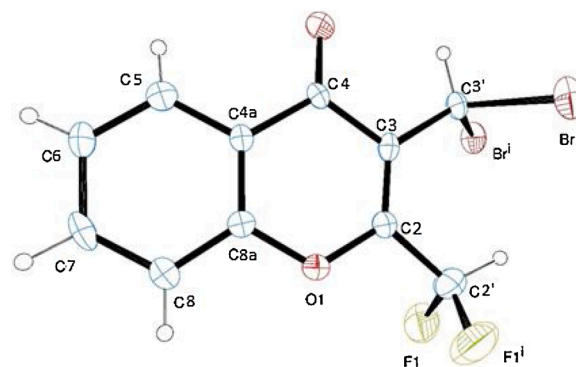
Table 2

Experimental and calculated electronic spectra of 1 – 7, and tentative assignment of the absorption bands.

Comp.	Experimental ^[a]	Calculated ^[a,b] (B3LYP/ 6–311++G(d,p))	Tentative Assignment	$\Delta E_{\text{HOMO-LUMO}}^{[d]}$
1	205	205 (0.147)	HOMO-3→LUMO + 1 (56 %)	4.53
		206 (0.207)	HOMO-2→LUMO + 1 (80 %)	
	230	242 (0.487)	HOMO → LUMO + 1 (56 %)	
	250 ^[c]	246 (0.100)	HOMO-3→LUMO (82 %)	
	319	308 (0.111)	HOMO → LUMO (94 %)	
2		202 (0.307)	HOMO-1→LUMO + 2 (54 %)	4.35
	205	204 (0.091)	HOMO-2→LUMO + 3 (88 %)	
	224	211 (0.228)	HOMO-3→LUMO + 1 (41 %)	
	246	255 (0.460)	HOMO → LUMO + 1 (49 %)	
	252 ^[c]	261 (0.091)	HOMO-3→LUMO (50 %)	
	309	323 (0.094)	HOMO → LUMO (96 %)	
	202 ^[c]	213 (0.279)	HOMO → LUMO + 2 (50 %)	
3	209	219 (0.444)	HOMO-5→LUMO + 1 (36 %)	4.45
			HOMO-3→LUMO + 1 (32 %)	
			HOMO-4→LUMO (37 %)	
	237	262 (0.282)	HOMO-3→LUMO (36 %)	
	318	316 (0.134)	HOMO → LUMO (95 %)	
4		211 (0.132)	HOMO → LUMO + 1 (45 %)	4.67
	205	214 (0.205)	HOMO-5→LUMO + 1 (55 %)	
		223 (0.196)	HOMO-2→LUMO + 1 (55 %)	
	235	256 (0.143)	HOMO-3→LUMO (29 %)	
		259 (0.075)	HOMO-4→LUMO (76 %)	
	250 ^[c]	261 (0.149)	HOMO-2→LUMO (37 %)	
		300 (0.104)	HOMO → LUMO (90 %)	
	201	206 (0.212)	HOMO → LUMO + 3 (74 %)	
	216 ^[c]	219 (0.275)	HOMO-7→LUMO (36 %)	
		230 (0.164)	HOMO-2→LUMO + 1 (56 %)	
5		253 (0.092)	HOMO-4→LUMO (57 %)	4.56
	276	266 (0.165)	HOMO → LUMO + 1 (55 %)	
	340	309 (0.121)	HOMO → LUMO (94 %)	
		210 (0.203)	HOMO → LUMO + 3 (66 %)	
6	202	221 (0.243)	HOMO-9→LUMO (57 %)	4.48
		230 (0.124)	HOMO-2→LUMO + 1 (35 %)	
	241	261 (0.148)	HOMO-4→LUMO (58 %)	
	252 ^[c]	270 (0.157)	HOMO → LUMO + 1 (60 %)	
	306	317 (0.101)		

Table 2 (continued)

Comp.	Experimental ^[a]	Calculated ^[a,b] (B3LYP/ 6–311++G(d,p))	Tentative Assignment	$\Delta E_{\text{HOMO-LUMO}}^{[d]}$
7		208 (0.148)	HOMO → LUMO (95 %)	4.55
	205	213 (0.245)	HOMO → LUMO + 2 (54 %)	
	228	224 (0.209)	HOMO-5→LUMO + 1 (47 %)	
	249 ^[c]	262 (0.257)	HOMO-2→LUMO + 1 (41 %)	
	306	310 (0.100)	HOMO → LUMO + 1 (70 %)	
			HOMO → LUMO (90 %)	

**Fig. 1.** View of 3-dibromomethyl-2-difluoromethyl chromone (**5**) showing the labeling of the non-H atoms and their displacement ellipsoids at the 30 % probability level. Symmetry operation (i) x, -y+1/2, z.

the $\pi \cdots \pi$ stacking interaction (red circle). Moreover, I, II and IV exhibit spikes attributed to F \cdots H, Br \cdots H and O \cdots Br contacts, respectively. The —CF₂H and CHBr—₂ groups with 25.5 % and 28.2 % contribution to the total HS for the F \cdots H and Br \cdots H interactions, respectively, contribute to stabilize the supramolecular self-assembly.

2.5. AIM and NCI analysis of weak interactions for **5**

The AIM approach was used to extend the analysis and characterization of the weak intermolecular interactions of **5**. The Fig. 6 show a tetramer of **5**, where the main critical points (CPs) of bond between molecules are illustrated (Fig. 6a). Besides, the Laplacian ($\nabla^2 \rho$) of the (b) C—Br \cdots OC, (c) CF \cdots H-C and (d) CH \cdots OC— (intra) contacts, respectively are depicted. On the other hand, the topological parameters that are considered to explore the character and type of intermolecular interaction are listed in Table 5.

QTAIM parameters at the bond critical point (CPs) such as electron density [$\rho(r)$], its Laplacian [$\nabla^2 \rho$], the Lagrangian kinetic energy [$G(r)$] and virial field function [$V(r)$] characterize efficiently chemical bonds and weak interactions[46]. According to topological criteria proposed by Koch and Popelier[47], [CP1] and [CP3] on the one hand and [CP2], [CP4] and [CP5], by the other hand, can be classified as interactions with moderate and low electron density values, respectively.

The $\rho(r)$ is associated with the bond strength or bond order with values between 0.002 and -0.034 au. In **5**, all values of the Laplacian exhibit negative values ($\nabla^2 \rho < 0$), suggesting covalent nature open-shell interactions[48]. In the Fig. 6 (b – d) the contour Laplacian maps of the charge density of Br \cdots O, H \cdots F and H \cdots O interactions are depicted. The Br \cdots O contact evidence regions of charge depletion (Fig. 6c, red arrow), that are describe as σ -hole in OCCH₃ \cdots Br and COCH₃ \cdots CCl₃ of

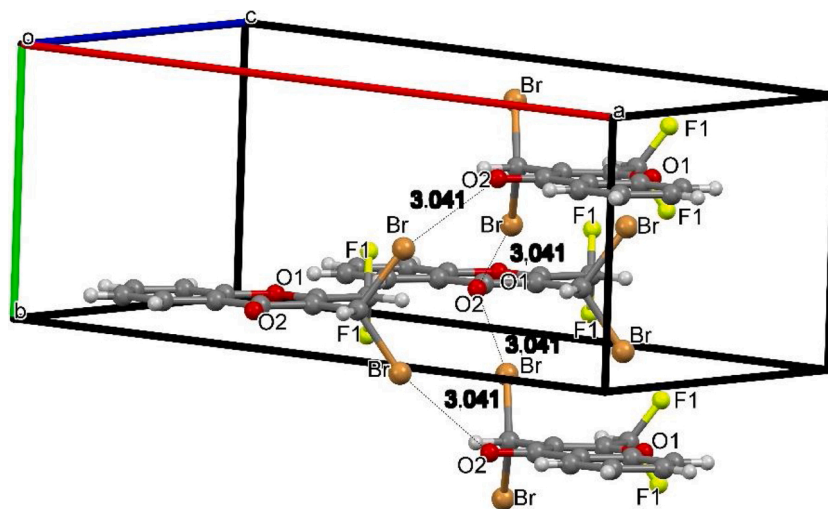


Fig. 2. Packing diagram of **5** via $C_{sp^2}\text{-O}\cdots\text{Br-C}_{sp^3}$ intermolecular interactions (dotted lines).

heterodimeric complexes[49]. Likewise, the electron density distribution involving $\text{H}\cdots\text{F}$ and $\text{H}\cdots\text{O}$ interactions [Fig. 6 (c – d), blue arrow] shows regions of charge depletion and concentrations in the F and O atoms, respectively[50].

The non-covalent interactions (NCI) method[51] was carried out in the tetramer of **5** to complete the intermolecular interaction analysis. The reduced density gradient (RDG) isosurfaces reveals weak interaction regions. The interaction types, are distinguished with a bar of colors (Fig. 7d) as strong attraction (blue color), Van der Waals interactions (green color) and strong repulsion (red color) zones. RDG predicts mainly green isosurfaces between molecules of tetramer of **5** that can be interpreted as Van der Waals interactions (Fig. 7, green circle). The $\text{C-H}\cdots\text{O-C}$ intramolecular contact shows a weak attractive character, suggesting a weak H-bond (Fig. 7, blue circle). In addition, it is evidenced a large RDG isosurfaces in the $\text{F}_2\text{C-H}\cdots\text{Br-C}$ intramolecular contact between $-\text{CHF}_2$ and $-\text{CHBr}_2$ groups. Although, the intermolecular $\text{F}\cdots\text{H}$ contacts show low RDG isosurfaces both fluorine atoms exert through their withdrawing electron effect, a higher acidity of the H-CF_2 -proton providing a suitable environment for the $\text{F}_2\text{C-H}\cdots\text{Br-C}$ intramolecular interaction.

3. Conclusions

Seven new halo-chromones were synthesized employing mild reaction conditions showing moderate to high yields. The intermolecular interactions in the solid of **1–7** were detected in the vibrational spectra. The shift of the $\text{C}=\text{O}$ bands towards lower frequencies could be attributed to close contacts such as $\text{C}_{sp^2}\text{-O}\cdots\text{Br-C}_{sp^3}$. For all compounds, the transitions between the frontier molecular orbitals (HOMO \rightarrow LUMO) are attributed to $\pi \rightarrow \pi^*$ excitations involving the whole molecules. The energy gap between the HOMO/LUMO orbitals showed an effect of stabilization of the bromine and chlorine atoms at C-6 and C-3 of the **1–3** compounds.

Hirshfeld analysis of **5** suggests that the halogen atoms are involved in several non-covalent interactions in solid state. AIM and NCI analysis of weak interactions of **5** complement this study revealing through RDG isosurfaces $\text{C-H}\cdots\text{Br-C}$ (intra), $\text{C-Br}\cdots\text{Br-C}$, $\text{CH}\cdots\text{O-C}$, $\text{CF}\cdots\text{H-C}$, $\text{C-F}\cdots\text{Br-C}$ and $\text{CH}\cdots\text{Br-C}$ (intra) inter/intra molecular interactions.

These results show that fluorine atoms are relevant not only for their contribution to the stabilization of the supramolecular crystalline assembly, with intermolecular $\text{F}\cdots\text{H}$ interactions as was stated in section 2.3, but also for promoting the conformation that the molecule finally adopts due to the intermolecular $\text{F}_2\text{C-H}\cdots\text{Br-C}$ interaction as discussed from NCI analysis.

In view of the observed results, the contribution of fluorine atoms in this class of heterocyclic compounds deserves in our opinion, further attention.

4. Experimental section

4.1. Instrumentation

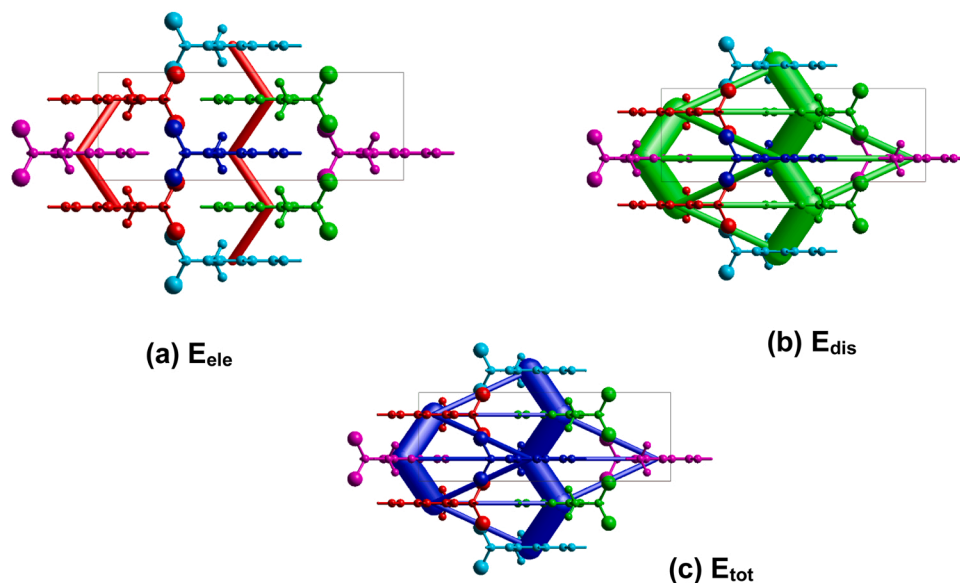
The melting points were determined on a Büchi Melting Point M-560. Infrared absorption spectra (KBr disks) were recorded on a Varian 660-IR FT-IR spectrometer with a resolution of 2 cm^{-1} in the range from 4000 to 400 cm^{-1} (see Fig. S1). The Raman dispersion spectra of the solids were measured in the $3500\text{--}100\text{ cm}^{-1}$ range with a Thermo-scientific DXR Raman microscope, using a diode pump and solid-state laser of $\lambda = 780\text{ nm}$, with spectral resolution of 5 cm^{-1} (see Fig. S2). The ^1H , ^{19}F and ^{13}C NMR spectra were recorded at $25\text{ }^\circ\text{C}$ on a Bruker Avance II 500, Bruker AV 300 (300 MHz), and Bruker AV 400 (400 MHz) spectrometers using CDCl_3 as solvent. Chemical shifts (δ) are expressed in ppm relative to TMS for ^1H and ^{13}C and TFA ($\delta = -71.0\text{ ppm}$) for ^{19}F (see Figs. S3–8). Coupling constants (J) are reported in Hz, and the multiplicity was signalized as: s (singlet), d (doublet), dd (double doublet), ddd (double double doublet), t (triplet), q (quartet). The experimental and calculated ^1H and ^{13}C chemical shifts of **1–7** are shown in Error! Reference source not found.S1. Electronic spectra were measured on a Varian 50 BIO UV-vis spectrophotometer at 2.0 nm spectral bandwidth using methanol as solvent (see Fig. S10). GS-MS determinations were obtained using a chromatograph (Agilent Technologies 7890 A) coupled to a mass selective detector (Agilent Technologies 5975 C). The electron energy was 70 eV with a mass range of $50\text{--}500\text{ amu}$ and a pressure in the mass spectrometer lower than 10^{-5} Torr . The mass spectra are shown in Fig. S11.

4.2. Synthesis of chromones **1** and **2**

6-Chloro-3-methyl-2-trifluoromethyl chromone (**1**). In a reactor provided with a condenser adapted for single distillation, 2.6 mL (22.4 mmol) of benzoyl chloride and 1.6 mL (21.4 mmol) of propanoic acid were heated from $20\text{ }^\circ\text{C}$ to $130\text{ }^\circ\text{C}$ under stirring for two hours. The propionyl chloride was distilled and used as obtained in the next step. 2-Hydroxy-5-chloropropiophenone was prepared by esterification of 1.2 mL (12.2 mmol) of p-chlorophenol, 1.4 mL (15.6 mmol) of propionyl chloride and 0.5 mL of pyridine. The mixture was stirred at room temperature during 1 h . The propionyl ester of chlorophenol was isolated from the reaction mixture from distillation and used as obtained in the

Table 3

Energy frameworks for **5**, showing the interaction energies (a) electrostatic, (b) dispersion and (c) total interaction energy (kJ/mol). Selected intra- and intermolecular contacts [\AA and $^\circ$] and $\pi\cdots\pi$ staking between centroids.



C ^a	D-X...A-Y Contact ^b	D-X / A-Y	d(X...A)	\angle D-X...A	R ^c	E _{ele}	E _{pol}	E _{dis}	E _{rep}	E _{tot}
■	C3'-Br...O2-C4 ⁱ	1.933 / 1.215	3.0415(2)	160.93(1)	7.00	-6.0	-0.9	-16.1	11.9	-11.6
	C3'-Br...O2-C4 ⁱⁱ	1.933 / 1.215	3.0415(2)	160.93(1)						
■	C4-O2...Br-C3 ⁱⁱⁱ	1.215 / 1.933	3.0415(2)	134.00(1)						
	C4-O2...Br-C3 ^{iv}	1.215 / 1.933	3.0415(2)	134.00(1)						
■	C12'-F1...H5-C5	1.337 / 0.791	2.933	105.45	8.63	-3.4	-1.1	-9.1	1.8	-11.0
■	Cg(1)···Cg(2)	-	3.651 ^d	-	7.63	-15.6	-1.7	-59.7	27.0	-48.8
	Cg(2)···Cg(2)	-	3.798 ^d	-						
■	C3'-Br...Br-C3 ^v	1.215 / 1.933	3.7978(3)	144.84(1)	6.96	2.2	-0.1	-7.8	3.8	-1.7
	C3'-H3'...O2-C4 (intra)	0.971 / 1.215	2.264	111.36						

^a Molecule color; ^b Symmetry transformations used to generate equivalent atoms: (i): 1/2-x,1-y,-1/2+z, (ii): 1/2-x,-1/2+y,-1/2+z, (iii): 1/2-x,1-y,1/2+z, (iv): 1/2-x,1/2+y,1/2+z, (v): x,1/2-y,z^c

^a Molecule color.

^b Symmetry transformations used to generate equivalent atoms: (i): 1/2-x,1-y,-1/2+z, (ii): 1/2-x,-1/2+y,-1/2+z, (iii): 1/2-x,1-y,1/2+z, (iv): 1/2-x,1/2+y,1/2+z, (v): x,1/2-y,z.

^c distance between molecular centroids (mean atomic position) in \AA .

^d Interplanar chromone distance of nearest neighbor molecules, in \AA .

next step. All the product was used in the subsequent Fries rearrangement adding 0.220 g (1.65 mmol) of AlCl_3 and heating the mixture at 140°C during 2 h to obtain, after treatment with 6 N hydrochloric acid and product isolation, the desired 2-hydroxy-5-chloropropiophenone. In the last step, this compound was subjected to one-pot cyclocondensation with trifluoroacetic anhydride as previously reported [32]. White crystals (recrystallized twice from hot hexane); m.p. $89\text{--}90^\circ\text{C}$; 45 % yield; UV (MeOH): 205, 230, 250, 319 nm; IR (KBr): 1649, 1606, 1173, 1149, 731, 680, 533 cm^{-1} ; ^1H NMR (CDCl_3 , 300 MHz): δ 8.14 (d, $J = 2.5$ Hz, H-5), 7.66 (dd, $J = 9$ and 2.5 Hz, H-7), 7.46 (d, $J = 9$ Hz, H-8), 2.22, (q, $^5J_{\text{H,F}} = 2$ Hz, CH_3); ^{13}C NMR (63 MHz, CDCl_3) δ 176.9 (C-4), 153.4

(C8a), 148.5 (q, $J = 37$ Hz, C-2), 135.0 (C-7), 132.0 (C-6), 125.5 (C-5), 123.3 (C-4a), 121.1 (q, $J = 1$ Hz, C-3), 120.1 (C-8), 119.8 (q, $J = 276$ Hz, CF_3), 8.8 (q, $^5J_{\text{C,F}} = 2$ Hz, CH_3); ^{19}F NMR (282 MHz, CDCl_3) δ -65.35 (s, CF_3); GC-MS, 70 eV, m/z , (rel. int.): 264, (36), $[\text{M} + 2]^+$; 263, (7), $[\text{M} + 1]^+$; 262, (100), $[\text{M}]^+$; 243, (5), $[\text{M-F}]^+$; 227, (3), $[\text{M-Cl}]^+$; 193, (99), $[\text{M-CF}_3]^+$ (Scheme 2).

3,6-dibromo-2-trifluoromethyl chromone (**2**). To a vigorously stirred solution of 0.2292 g (1.1 mmol) of 2-trifluoromethylchromone in glacial acetic acid (2.7 mL) maintained at 20°C , bromine (3.5 mL, 68.3 mmol) was slowly added dropwise. The resulting mixture was refluxed for 24 h, and after cooling, the obtained precipitate was filtered off, washed

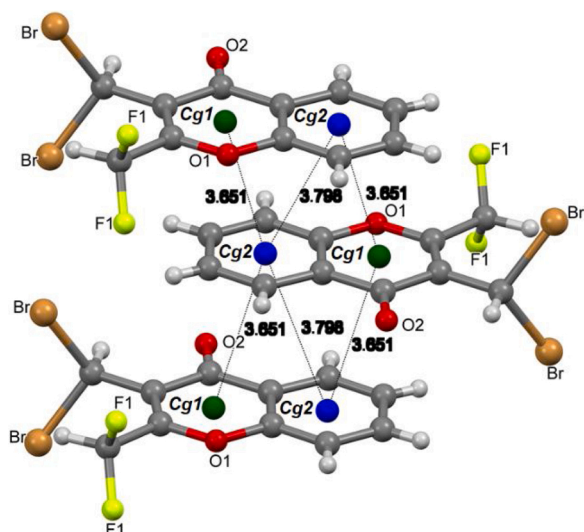


Fig. 3. View of the $\pi\cdots\pi$ stacking, showing the intercentroids distances for **5**.

Table 4

Geometrical parameters for the π -stacking moieties involved in the $\pi\cdots\pi$ interactions for **5** (Å, °).

Rings I - J ^a	Cg(I) ...Cg (J) ^b	Cg(I) ...Perp ^c	Cg(J) ...Perp ^d	α^e	β^f	γ^g	symmetry
Cg (1)...	3.6511 (3)	3.4790	3.4790	0.00	17.7	17.7	-x,-1/ 2+y,2-z
Cg (2)	3.7977 (3)	3.4790	3.4790	0.00	23.6	23.6	-x,-1/ 2+y,2-z

^a Cg(1) and Cg(2) are the centroids of pyrane and benzene rings, respectively.

^b Centroid distance between ring i and ring J.

^c Perpendicular distance of Cg(I) on ring J (Å).

^d Perpendicular distance of Cg(J) on ring I (Å).

^e Dihedral angle between planes I and J (Degrees).

^f Angle between the centroid vector Cg(i) \cdots Cg(j) and the normal to the plane

(i).

^g Angle between the centroid vector Cg(i) \cdots Cg(j) and the normal to the plane

(j).

thoroughly with water and then dried to constant weight in vacuum (Scheme 2). The crude product was purified by column chromatography (Hexane/EtOAc, 7:3) to give 158.5 mg (40 %) of **2** as a white crystalline solid. UV (MeOH): 205, 224, 246, 252, 309 nm; IR (KBr): 1657, 1613, 1177, 1157, 725, 663, 607 cm^{-1} ; ^1H NMR (300 MHz, CDCl_3): δ 8.38 (dd, $J = 2.5$ and 0.4 Hz, H-5), 7.89 (dd, $J = 9$ and 2.5 Hz, H-7), 7.48 (dd, $J = 9$ and 0.4 Hz, H-8); ^{13}C NMR (151 MHz, CDCl_3): δ 171.1 (C-4), 153.5 (C-8a), 150.0 (q, $J = 38$ Hz, C-2), 138.6 (C-7), 129.3 (C-5), 122.9 (C-4a or C-6), 120.7 (C-4a or C-6), 120.3 (C-8), 118.9 (q, $J = 277$ Hz, CF_3), 111.0 (d, $J = 1$ Hz, C-3); ^{19}F NMR (282 MHz, CDCl_3): δ -66.29 (s, CF_3); GC-MS, 70 eV, m/z , (rel. int.): 374, (50), $[\text{M} + 4]^+$; 372, (100), $[\text{M} + 2]^+$; 370, (50), $[\text{M}]^+$; 291, (3), $[\text{M}-^{79}\text{Br}]^+$.

4.3. General procedure for bromination of 3-methyl-2-polyhaloalkyl chromone (synthesis of 3-7)

In a bottom flask with ground glass joint, 3-methyl-2-polyhaloalkyl chromone (1.5 mmol) was dissolved in 10 mL of carbon tetrachloride. Then, 10 mL of aqueous saturated bromine solution was added, the mixture was sealed with a rubber stopper and kept with stirring at room temperature under visible light irradiation for 1–6 days (monitored by

TLC). The organic phase was separated, dried (over Na_2SO_4) and the solvent removed with a rotary evaporator.

Compound **5** is a reaction side product, isolated by column chromatography (Hexane/EtOAc, 9:1) during the purification of **4**. The stoichiometric detail is described in Fig. S15 of the supplementary material.

4.3.1. 3-bromomethyl-6-chloro-2-trifluoromethyl chromone (**3**)

White crystalline solid (250 mg, 80 %) m.p. 97–99 °C; UV (MeOH): 202, 209, 237, 318 nm; IR (KBr): 1649, 1606, 1173, 1149, 1033, 731, 680, 633 cm^{-1} ; ^1H NMR (CDCl_3 , 300 MHz): δ 8.19 (d, $J = 2.5$ Hz, H-5), 7.72 (dd, $J = 9$ Hz and $J = 2.5$ Hz, H-7), 7.52 (d, $J = 9$ Hz, H-8), 4.53 (br. quint, $^5J_{\text{H,F}} = 1$ Hz, CH_2Br); ^{13}C NMR (63 MHz, CDCl_3): δ 174.5 (C-4), 153.3 (C-8a), 150.1 (q, $J = 38$ Hz, C-2), 135.7 (C-7), 132.9 (C-6), 125.9 (C-5), 123.6 (C-4a), 121.4 (br. q, $J = 1$ Hz, C-3), 120.2 (C-8), 119.9 (q, $J = 277$ Hz, CF_3), 18.8 (q, $J = 3$ Hz, CH_2Br); ^{19}F NMR (282 MHz, CDCl_3): δ -65.5 (s, CF_3); GC-MS, 70 eV, m/z , (rel. int.): 342, (15), $[\text{M} + 2]^+$; 340, (11), $[\text{M}]^+$; 261, (100), $[\text{M}-^{79}\text{Br}]^+$; 226, (4), $[\text{M}-^{79}\text{Br}^{35}\text{Cl}]^+$.

4.3.2. 3-bromomethyl-2-difluoromethyl chromone (**4**)

White solid (345 mg, 84 %) m.p. 112–114 °C; UV (MeOH): 205, 235, 250, 303 nm; IR (KBr): 3022, 2922, 1649, 1609, 1432, 1056, 609 cm^{-1} ; ^1H NMR (600 MHz, CDCl_3): δ 8.24 (ddd, $J = 8$, 1.8 and 0.4 Hz, H-5), 7.75 (ddd, $J = 8.5$, 7 and 1.5 Hz, H-7), 7.52 (ddd, $J = 8.5$, 1 and 0.4 Hz, H-8), 7.48 (ddd, $J = 8$, 7 and 1 Hz, H-6), 6.78 (t, $^2J_{\text{H,F}} = 52.4$ Hz, CF_2H), 4.57 (t, $^5J_{\text{H,F}} = 1$ Hz, CH_2Br); ^{13}C NMR (151 MHz, CDCl_3): δ 175.7 (C-4), 155.4 (C-8a), 154.6 (t, $^2J_{\text{C,F}} = 25$ Hz, C-2), 135.1 (C-7), 126.44 (C-5 or C-6), 126.41 (C-5 or C-6), 123.1 (C-4a), 121.3 (t, $^3J_{\text{C,F}} = 2.5$ Hz, C-3), 118.5 (C-8), 109.6 (t, $^1J_{\text{C,F}} = 244$ Hz, CF_2H), 18.9 (t, $^4J_{\text{C,F}} = 1.5$ Hz, CH_2Br); ^{19}F NMR (565 MHz, CDCl_3): δ -120.58 (CF_2H); GC-MS, 70 eV, m/z , (rel. int.): 290, (13), $[\text{M} + \text{H}]^+$; 288, (13), $[\text{M}]^+$; 209, (100), $[\text{M}-\text{Br}]^+$.

4.3.3. 3-dibromomethyl-2-difluoromethyl chromone (**5**)

White solid (30 mg, 6%); UV (MeOH): 201, 216, 276, 340 nm; IR (KBr): 3010, 2922, 1650, 1637, 1068, 646, 600 cm^{-1} . GC-MS, 70 eV, m/z , (rel. int.): 366, (7), $[\text{M}]^+$; 368, (14), $[\text{M} + 2]^+$; 370, (7), $[\text{M} + 4]^+$; 287, (100), $[\text{M}-\text{Br}]^+$.

4.3.4. 3-dibromomethyl-2-dichloromethyl chromone (**6**)

Yellow solid (23 mg, 20 %) m.p. 229–232 °C; UV (MeOH): 202, 241, 252, 306 nm; IR (KBr): 3040, 3010, 1647, 1625, 763, 633, 587 cm^{-1} ; ^1H NMR (600 MHz, CDCl_3): δ 8.22 (dd, $J = 8$, 1.5 Hz, H-5), 7.79 (ddd, $J = 8.5$, 7 and 1.5 Hz, H-7), 7.71 (br. s., CHBr_2), 7.62 (d, $J = 8.5$ Hz, H-8), 7.49 (ddd, $J = 8$, 7 and 1 Hz, H-6), 7.39 (s, CHCl_2); ^{13}C NMR (151 MHz, CDCl_3): δ 155.62 (C-2); 135.44 (C-7); 126.76 (C-5); 126.56 (C-6); 122.37 (C-4a); 118.50 (C-8); 63.36 (CCH_2H); 25.07 (CHBr_2). GC-MS, 70 eV, m/z , (rel. int.): 398, (1), $[\text{M}]^+$; 400, (4), $[\text{M} + 2]^+$; 402, (3), $[\text{M} + 4]^+$; 404, (1), $[\text{M} + 6]^+$; 321, (100), $[\text{M}-\text{Br}]^+$.

4.3.5. 3-bromomethyl-2-pentafluoroethyl chromone (**7**)

White solid (412 mg, 80 %) m.p. 83–85 °C; UV (MeOH): 205, 228, 249, 306 nm; IR (KBr): 2852, 1657, 1630, 1435, 1204, 1164, 607 cm^{-1} ; ^1H NMR (600 MHz, CDCl_3): δ 8.26 (ddd, $J = 8$, 1.5 and 0.5 Hz, H-5), 7.79 (ddd, $J = 8.5$, 7 and 1.5 Hz, H-7), 7.52 (ddd, $J = 8.5$, 1 and 0.5 Hz, H-8), 7.51 (ddd, $J = 8$, 7 and 1 Hz, H-6), 4.58 (t, $^5J_{\text{H,F}} = 2$ Hz, CH_2Br); ^{13}C NMR (151 MHz, CDCl_3): δ 175.3 (C-4), 155.2 (C-8a), 149.4 (t, $^2J_{\text{C,F}} = 28$ Hz, C-2), 135.5 (C-7), 126.8 (C-5 or C-6), 126.8 (C-5 or C-6), 124.0 (C-4a), 122.6 (C-3), 118.5 (qt, $J = 287$, 35.5 Hz, CF_2CF_3), 118.4 (C-8), 18.94 (t, $^4J_{\text{C,F}} = 5.5$ Hz, CH_2Br); ^{19}F NMR (565 MHz, CDCl_3): δ -116.07 (CF_2) -82.86 (CF_3); GC-MS, 70 eV, m/z , (rel. int.): 356, (19), $[\text{M}]^+$; 358, (18), $[\text{M} + 2]^+$; 277, (100), $[\text{M}-\text{Br}]^+$.

4.4. X ray diffraction data and structural refinement of **5**

The measurements were performed on an Oxford Xcalibur Gemini,

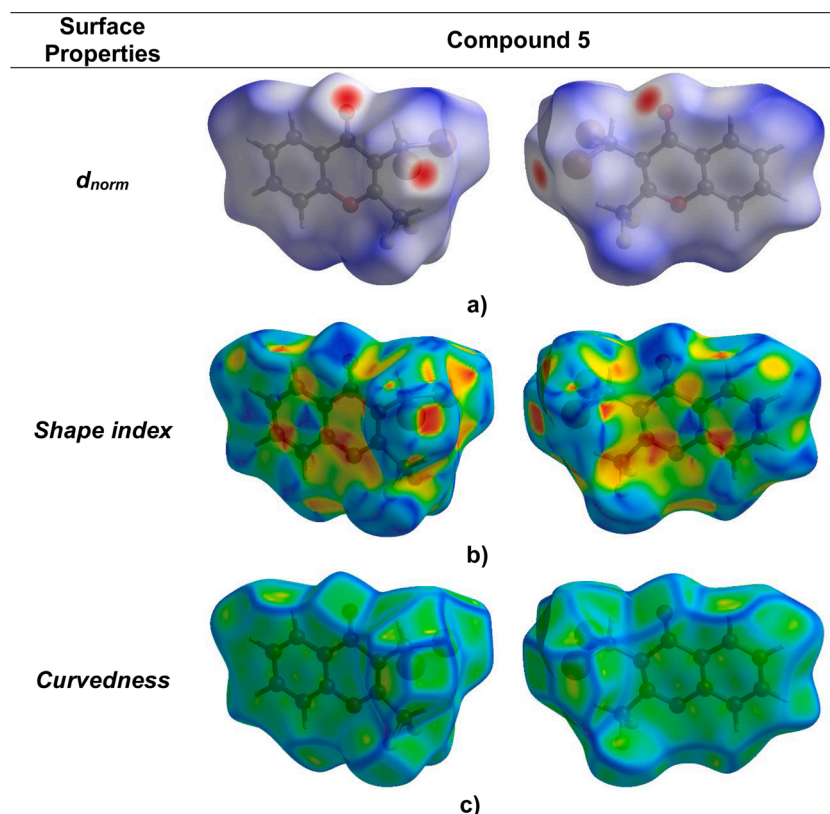


Fig. 4. Hirshfeld surfaces mapped over d_{norm} , shape index and curvedness index of 5.

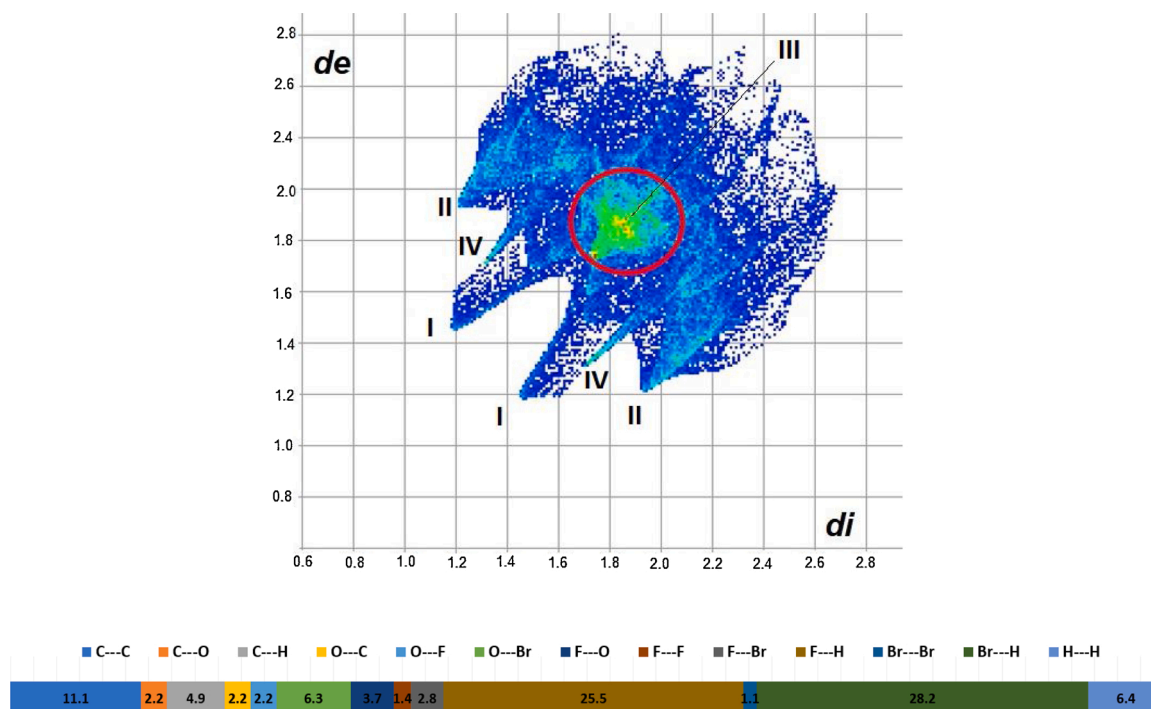
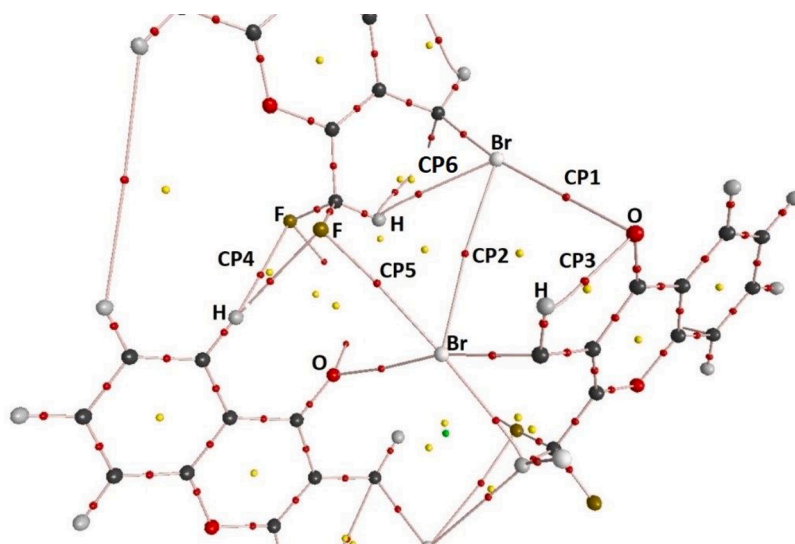


Fig. 5. Top: 2D-Fingerprint plot of 5. Close contacts are labeled as I: F...H, II: Br...H, III: C...C, IV: O...Br. Bottom: Relative contribution (%) of intermolecular contacts to the Hirshfeld surface area of 5.

Eos CCD diffractometer with graphite-monochromated MoK α ($\lambda = 0.71073 \text{ \AA}$) radiation. X-ray diffraction intensities were collected (ω scans with ϑ and κ -offsets), integrated and scaled with CrysAlisPro[52] suite of programs. The unit cell parameters were obtained by

least-squares refinement (based on the angular setting for all collected reflections with intensities larger than seven times the standard deviation of measurement errors) using CrysAlisPro. Data were corrected empirically for absorption employing the multi-scan method



(a) Critical points (CPs) of bond

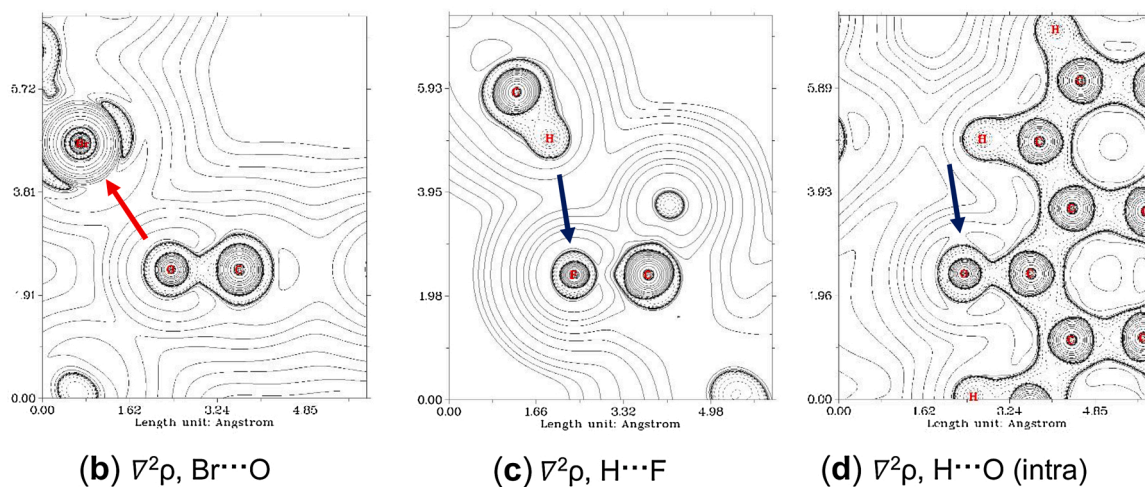
(b) $\nabla^2\rho$, Br...O(c) $\nabla^2\rho$, H...F(d) $\nabla^2\rho$, H...O (intra)

Fig. 6. (a) AIM distribution of bond, ring and cage critical points (red, yellow and green spheres, respectively) and bond paths for the tetramer of compound 5. (b - d) Contour plot of Laplacian of electron density of the Br...O, H...F and H...O interactions of 5. (For interpretation of the references to colour in this figure legend, the reader is referred to the web version of this article).

Table 5

QTAIM $\rho(r)$, $\nabla^2\rho$, $V(r)$ and $G(r)$ parameters at the bond CPs labelled in Fig. 6 in a.u.

Interaction	CP	$\rho(r)$	$\nabla^2\rho$	$V(r)$	$G(r)$
C—Br...O—C	CP1	0.0147	-0.0145	0.0108	0.0126
C—Br...Br—C	CP2	0.0037	-0.0024	0.0016	0.0020
C—H...OC— (intra)	CP3	0.0129	-0.0157	0.0104	0.0130
C—F...H—C	CP4	0.0049	-0.0060	0.0031	0.0045
C—F...Br—C	CP5	0.0054	-0.0058	0.0035	0.0047
C—H...BrC— (intra)	CP6	0.0111	-0.0098	0.0065	0.0081

implemented in CrysAlisPro. The non-H structures were solved by the intrinsic phasing procedure implemented in SHELXT[53] and the molecular model refined by full-matrix least-squares with SHELXL of the SHELX suite of programs[54]. The hydrogen atoms were determined in a Fourier difference map phased on the heavier atoms and refined at their found positions with isotropic displacement parameters. Crystal data and structure refinement results are summarized in Table S2.

Crystallographic structural data have been deposited at the Cambridge Crystallographic Data Centre (CCDC). Any request to the Cambridge Crystallographic Data Centre for this material should quote the full literature citation and the reference number CCDC 1972320.

4.5. Computational details

Quantum chemical calculations were performed for the ground state (gas phase) of 1–7 with the program package Gaussian 16[55]. Scans of the potential energy surface were carried out with the B3LYP/6-311++g(d,p) level of theory. Potential energy curves were performed around the dihedral angles involving the heavy bromine, chlorine and fluorine atoms (C3C2-C2'F, C2C3-C3'Br and C2C3-C3'Cl) (see Fig. S12).

For the geometry optimizations and vibrational frequency calculations Density Functional Theory (B3LYP) method employing the 6-311++G(d,p) basis set was used. In all cases, the calculated vibrational properties correspond to potential energy minima with no imaginary values for the frequencies. The ^1H and ^{13}C chemical shifts (1–7), for the resultant B3LYP/6-311++g(2d,p) optimized geometries, were calculated

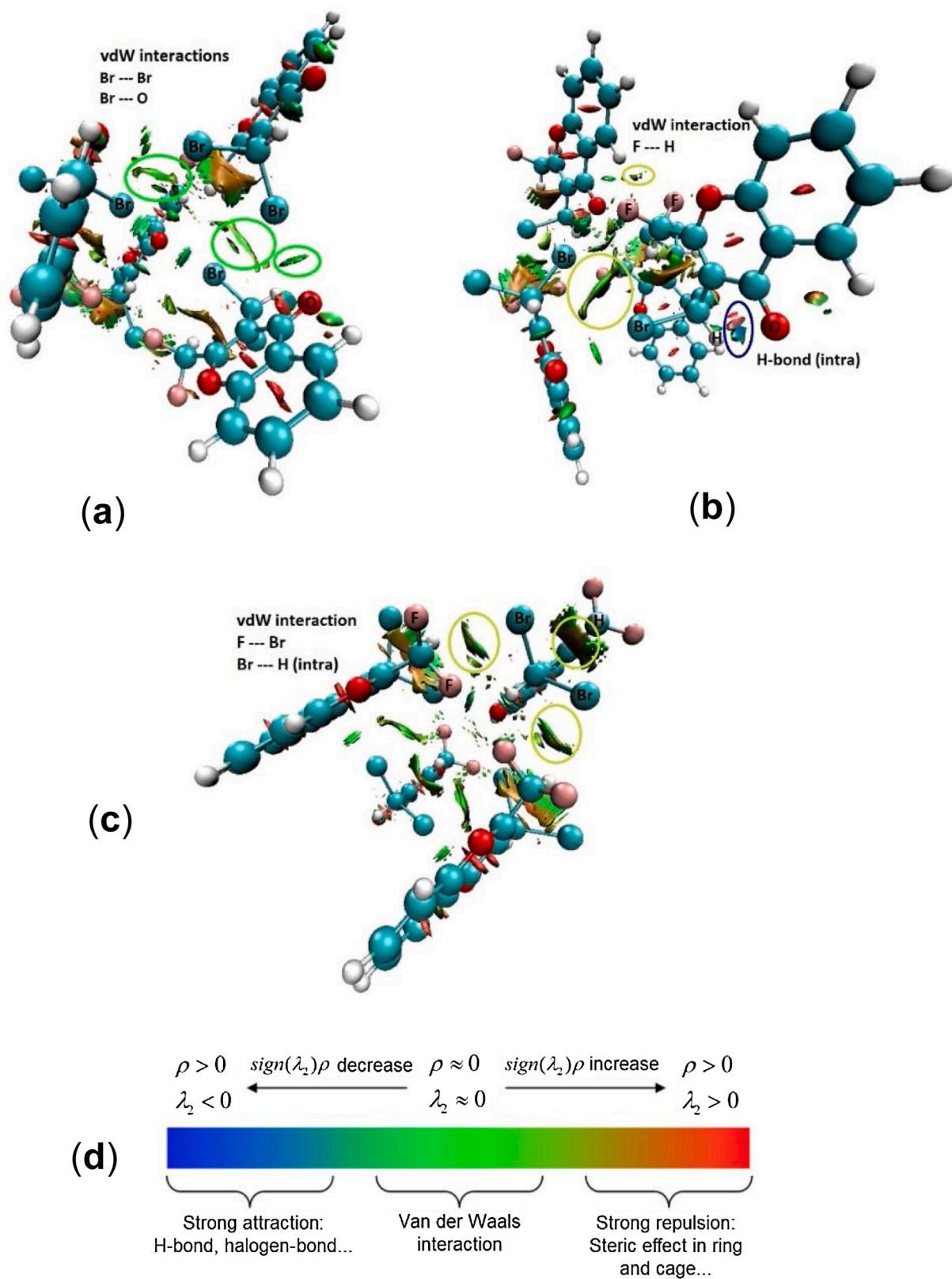
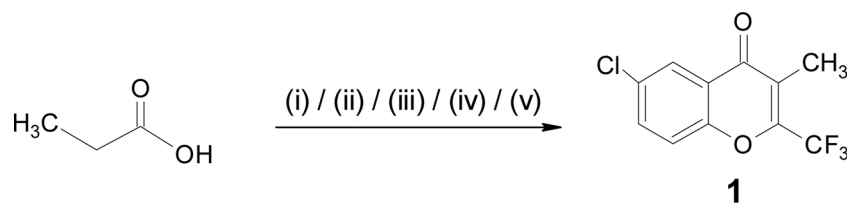


Fig. 7. NCI plots of 5, that show views of the weak interaction in the tetramer.

with the GIAO method (Gauge Including Atomic Orbital) using the corresponding TMS shielding calculated at the same level of theory. The electronic transitions were calculated with the Time-Dependent Density Functional Theory (TD-DFT)[55] taking into account implicitly the solvent effect (methanol).

4.6. Hirshfeld surface calculations of 5

The 2D-fingerprint plots of the Hirshfeld surface, energy frameworks and lattice interaction energies of 5 was generated using CrystalExplorer v17.5 software[56]. The amount of each intermolecular interaction in



Scheme 2. Synthetic procedure of 1.

(i) benzoyl chloride, 2h, 60 °C. (ii) Propanoic acid, simple distillation, 130 °C. (iii) p-chlorophenol, pyridine, r.t. (iv) AlCl₃, 2h, 140 °C. (v) (CF₃CO)₂O, 7h, 120 °C.

the crystal was visualized and decoded from the 2D-fingerprint plot. The normalized distance to the surface (d_{norm}) based on d_i and d_e , that are contact distances normalized by the van der Waals (vdW) atomic radii, can be visualized by red spots on the surface (see, Fig. 5). In fact, the 3D d_{norm} surfaces are mapped over a fixed color scale of -0.243 au (red) -0.824 au (blue) Å, shape index in the color range of -1.0 au (concave) -1.0 au (convex) Å, and curvedness index in the range of $14-4.0$ au (flat) -0.4 au (singular) Å. The surface properties above mentioned (d_{norm} , shape and curvedness index) were used to identify planar stacking. Moreover, the intermolecular interaction energies of **5** were calculated using TONTO program, integrated in the Crystal Explorer v17.5 software[43]. The intermolecular interaction energies were obtained using CE-B3LYP model (B3LYP/6-31 G(d,p))[56].

Declaration of Competing Interest

The authors declare that they have no known competing financial interests or personal relationships that could have appeared to influence the work reported in this paper.

Acknowledgements

EGNO, CDAL, PMBV and DAZ thank Central University of Ecuador (Grant, cif-5-ce-fc-q-1) and Faculty of Chemical Sciences of Ecuador for financial support. We thank all the staff from the Formative Research Commission. J.H.M thank UTE University for the financial support. GAE, OEP, SEU and JLJ thank CONICET (Grant PIP 11220130100651CO and 0359) and UNLP (Grant 11/X709, 11/X830 and 11/X848) of Argentina for financial support. GAE, OEP and SEU are Research Fellows of CONICET. J.L.J is a research fellow of Comisión de Investigaciones Científicas de la Prov. de Buenos Aires (CIC).

Appendix A. Supplementary data

Supplementary material related to this article can be found, in the online version, at doi:<https://doi.org/10.1016/j.jfluchem.2020.109717>.

References

- [1] S. Burattini, H.M. Colquhoun, J.D. Fox, D. Friedmann, B.W. Greenland, P.J. F. Harris, W. Hayes, M.E. Mackay, S.J. Rowan, A self-repairing, supramolecular polymer system: healability as a consequence of donor-acceptor $\pi-\pi$ stacking interactions, *Chem. Commun. (Camb.)* (2009) 6717-6719, <https://doi.org/10.1039/B910648K>.
- [2] M. Irigoyen, J.M. Matxain, F. Ruipérez, Effect of molecular structure in the chain mobility of dichalcogenide-based polymers with self-healing capacity, *Polymers* 11 (2019), <https://doi.org/10.3390/polym11121960>.
- [3] G. Berger, P. Frangville, F. Meyer, Halogen bonding for molecular recognition: new developments in materials and biological sciences, *Chem. Commun. (Camb.)* 56 (2020) 4970-4981, <https://doi.org/10.1039/D0CC00841A>.
- [4] A.K.A. Jaini, L.B. Hughes, M.M. Kitimet, K.J. Ulep, M.C. Leopold, C.A. Parish, Halogen bonding interactions for aromatic and nonaromatic explosive detection, *ACS Sens.* 4 (2019) 389-397, <https://doi.org/10.1021/acssens.8b01246>.
- [5] C.D. Alcívar León, G.A. Echeverría, O.E. Piro, S.E. Ulic, J.L. Jios, J.A. Pereañez, I. C. Henaó Castañeda, H. Pérez, The role of non-covalent interactions in some 2-trifluoromethylchromones in the solid state, *New J. Chem.* 41 (2017) 14659-14674, <https://doi.org/10.1039/C7NJ00481H>.
- [6] C. Bissanz, B. Kuhn, M. Stahl, A medicinal chemist's guide to molecular interactions, *J. Med. Chem.* 53 (2010) 5061-5084, <https://doi.org/10.1021/jm100112j>.
- [7] P. Politzer, J.S. Murray, T. Clark, Halogen bonding: an electrostatically-driven highly directional noncovalent interaction, *Phys. Chem. Chem. Phys.* 12 (2010) 7748-7757, <https://doi.org/10.1039/C004189K>.
- [8] V. Cody, P. Murray-Rust, Iodine- \cdots X(O, N,S) intermolecular contacts: models of thyroid hormone-protein binding interactions using information from the Cambridge crystallographic data files, *J. Mol. Struct.* 112 (1984) 189-199, [https://doi.org/10.1016/0022-2860\(84\)85061-9](https://doi.org/10.1016/0022-2860(84)85061-9).
- [9] E. Parisini, P. Metrangolo, T. Pilati, G. Resnati, G. Terraneo, Halogen bonding in halocarbon-protein complexes: a structural survey, *Chem. Soc. Rev.* 40 (2011) 2267-2278, <https://doi.org/10.1039/C0CS00177E>.
- [10] V.Y. Sosnovskikh, B.I. Usachev, 2-Polyfluoroalkylchromones. 5. Nitration and chlorination of 2-trifluoromethylchromones, *Russ. Chem. Bull.* 49 (2000) 2074-2076, <https://doi.org/10.1023/A:1009544630187>.
- [11] M. Gao, X. Han, Y. Sun, H. Chen, Y. Yang, Y. Liu, H. Meng, Z. Gao, Y. Xu, Z. Zhang, J. Han, Overview of sesquiterpenes and chromones of agarwood originating from four main species of the genus *Aquilaria*, *RSC Adv.* 9 (2019) 4113-4130, <https://doi.org/10.1039/C8RA09409H>.
- [12] G.P. Ellis, Chemistry of heterocyclic compounds: chromenes, chromanones, and chromones, *Chem. Heterocycl. N. (N Y)* (1977) 1-1196, <https://doi.org/10.1002/9780470187012>.
- [13] R.S. Keri, S. Budagumpi, R.K. Pai, R.G. Balakrishna, Chromones as a privileged scaffold in drug discovery: a review, *Eur. J. Med. Chem.* 78 (2014) 340-374, <https://doi.org/10.1016/j.ejmech.2014.03.047>.
- [14] A. Gaspar, M.J. Matos, J. Garrido, E. Uriarte, F. Borges, Chromone: a valid scaffold in medicinal chemistry, *Chem. Rev.* 114 (2014) 4960-4992, <https://doi.org/10.1021/cr400265z>.
- [15] J.H. Kini, V.K. Pai, Y.D. Bodke, Design and synthesis of some chromone derivatives of biological importance: a greener approach, *Mater. Today Proc.* 4 (2017) 11894-11901, <https://doi.org/10.1016/j.matpr.2017.09.109>.
- [16] C.F.M. Silva, D.C.G.A. Pinto, A.M.S. Silva, Chromones: a promising ring system for new anti-inflammatory drugs, *ChemMedChem* 11 (2016) 2252-2260, <https://doi.org/10.1002/cmdc.201600359>.
- [17] J. Reis, A. Gaspar, N. Milhazes, F. Borges, Chromone as a privileged scaffold in drug discovery: recent advances, *J. Med. Chem.* 60 (2017) 7941-7957, <https://doi.org/10.1021/acs.jmedchem.6b01720>.
- [18] H.A. Tawfik, E.F. Ewies, W.S. El-Hamouly, Synthesis of chromones and their applications during the last ten years, *Int. J. Res. Pharm. Chem.* 4 (2015) 1046-1085, <https://doi.org/10.1002/chin.201513331>.
- [19] V.Y. Sosnovskikh, Synthesis and reactions of halogen-containing chromones, *Russ. Chem. Rev.* 72 (2003) 489-516, <https://doi.org/10.1070/RC2003v072n06ABEH000770>.
- [20] P. Jeschke, W. Krämer, U. Schirmer, M. Witschel, The halogen substituent effect, *Mod. Methods Crop Prot. Res. John Wiley & Sons*, 2013, p. 442.
- [21] M. Martínez-Cifuentes, B. Weiss-López, R. Araya-Maturana, Theoretical study about the effect of halogen substitution on the reactivity of antitumor 3-Formylchromones and their free radicals, *J. Chem.* 2017 (2017), 9254831, <https://doi.org/10.1155/2017/9254831>.
- [22] C. Beudot, M.P. De Méo, D. Dauzonne, R. Elias, M. Laget, H. Guiraud, G. Balansard, G. Duménil, Evaluation of the mutagenicity and antimutagenicity of forty-two 3-substituted flavones in the Ames test, *Mutat. Res. Toxicol. Environ. Mutagen.* 417 (1998) 141-153, [https://doi.org/10.1016/S1383-5718\(98\)00103-X](https://doi.org/10.1016/S1383-5718(98)00103-X).
- [23] Y. Chen, H.-R. Liu, H.-S. Liu, M. Cheng, P. Xia, K. Qian, P.-C. Wu, C.-Y. Lai, Y. Xia, Z.-Y. Yang, S.L. Morris-Natschke, K.-H. Lee, Antitumor agents 292. Design, synthesis and pharmacological study of S- and O-substituted 7-mercapto- or hydroxy-coumarins and chromones as potent cytotoxic agents, *Eur. J. Med. Chem.* 49 (2012) 74-85, <https://doi.org/10.1016/j.ejmech.2011.12.025>.
- [24] J. Lee, T. Park, S. Jeong, K.-H. Kim, C. Hong, 3-Hydroxychromones as cyclin-dependent kinase inhibitors: synthesis and biological evaluation, *Bioorg. Med. Chem. Lett.* 17 (2007) 1284-1287, <https://doi.org/10.1016/j.bmcl.2006.12.011>.
- [25] J.K. Lynch, J.C. Freeman, A.S. Judd, R. Iyengar, M. Mulhern, G. Zhao, J.J. Napier, D. Wodka, S. Brodjan, B.D. Dayton, D. Falls, C. Ogiela, R.M. Reilly, T.J. Campbell, J.S. Polakowski, L. Hernandez, K.C. Marsh, R. Shapiro, V. Knourek-Segel, B. Droz, E. Bush, M. Brune, L.C. Preusser, R.M. Fryer, G.A. Reinhart, K. Houseman, G. Diaz, A. Mikhail, J.T. Limberis, H.L. Sham, C.A. Collins, P.R. Kym, Optimization of Chromone-2-carboxamide melanin concentrating hormone receptor 1 antagonists: assessment of potency, efficacy, and cardiovascular safety, *J. Med. Chem.* 49 (2006) 6569-6584, <https://doi.org/10.1021/jm060683e>.

- [26] N.S. Joshi, A.A. Shaikh, A.P. Deshpande, B.K. Karale, S.B. Bhirud, C.H. Gill, Note Synthesis, characterization and antimicrobial activities of some fluorine containing, *Indian J. Chem.* 44 (2005) 422–425.
- [27] S.G. Jagadhani, S.G. Kundalikar, B.K. Karale, Synthesis, characterization and antimicrobial screening of some fluorinated chromones and Chlorochromones, *Orient. J. Chem.* 30 (2014) 2073–2076, <https://doi.org/10.13005/ojc/300475>.
- [28] S.M. Tome, A.M.S. Silva, C.M.M. Santos, Synthesis and transformation of halochromones, *Curr. Org. Synth.* 11 (2014) 317–341.
- [29] C. Santos, V. Silva, A. Silva, Synthesis of chromone-related pyrazole compounds, *Molecules* 22 (2017) 1665, <https://doi.org/10.3390/molecules22101665>.
- [30] K.V. Shcherbakov, Y.V. Burgart, V.I. Saloutin, O.N. Chupakhin, Polyfluorine-containing chromen-4-ones: synthesis and transformations, *Russ. Chem. Bull.* 65 (2016) 2151–2162, <https://doi.org/10.1007/s11172-016-1563-0>.
- [31] M. Rocha, D.M. Gil, G.A. Echeverría, O.E. Piro, J.L. Jios, S.E. Ulic, A new perfluoromethyl aminoone derivative and the role of the hydrogen bonding in the intra- and intermolecular interactions, *J. Fluor. Chem.* 208 (2018) 36–47, <https://doi.org/10.1016/j.jfluchem.2018.01.001>.
- [32] I.C. Heano Castañeda, S.E. Ulic, C.O. Della Védova, N. Metzler-Nolte, J.L. Jios, One-pot synthesis of 2-trifluoromethylchromones, *Tetrahedron Lett.* 52 (2011) 1436–1440, <https://doi.org/10.1016/j.tetlet.2011.01.045>.
- [33] C.D. Alcívar León, G.A. Echeverría, O.E. Piro, S.E. Ulic, J.L. Jios, M. Burgos Paci, G. A. Argüello, The role of halogen C–X1…X2–C contact on the preferred conformation of 2-perhalomethylchromones in solid state, *Chem. Phys.* 472 (2016) 142–155, <https://doi.org/10.1016/j.chemphys.2016.03.017>.
- [34] C.D. Alcívar León, G.A. Echeverría, O.E. Piro, S.E. Ulic, J.L. Jios, C.A. Luna Tapia, M.F. Mera Guzmán, New thiourea and urea derivatives containing trifluoromethyl- and bis-trifluoromethyl-4H-chromen-3-yl substituents, *Mol. Phys.* (2018), <https://doi.org/10.1080/00268976.2018.1514132>.
- [35] C.D. Alcívar León, G.A. Echeverría, O.E. Piro, S.E. Ulic, J.L. Jios, A detailed experimental and theoretical study of two novel substituted trifluoromethylchromones. The influence of the bulky bromine atom on the crystal packing, *Spectrochim. Acta Part A Mol. Biomol. Spectrosc.* 136 (2015) 1358–1370, <https://doi.org/10.1016/j.saa.2014.10.022>.
- [36] C.D. Alcívar León, L.A. Ramos Guerrero, P.M. Bonilla Valladares, G.A. Echeverría, O.E. Piro, S.E. Ulic, J.L. Jios, P. Langer, Synthesis and structural study of 2-(haloalkyl)-3-methylchromones, *Monatsh. Chem.* 150 (2019) 1929–1940, <https://doi.org/10.1007/s00706-019-02512-5>.
- [37] J. Bernstein, R.E. Davis, L. Shimon, N.-L. Chang, Patterns in hydrogen bonding: functionality and graph set analysis in crystals, *Angew. Chemie Int. Ed. English* 34 (1995) 1555–1573, <https://doi.org/10.1002/anie.199515551>.
- [38] G. Cavallo, P. Metrangolo, R. Milani, T. Pilati, A. Priimagi, G. Resnati, G. Terraneo, The halogen bond, *Chem. Rev.* 116 (2016) 2478–2601, <https://doi.org/10.1021/acs.chemrev.5b00484>.
- [39] M. Esrafil, M. Solimannejad, A theoretical survey on strength and characteristics of F…F, Br…O and Br…Br interactions in solid phase, *Phys. Chem. Res.* 1 (2013) 142–151, <https://doi.org/10.22036/pcr.2013.3298>.
- [40] G.R. Desiraju, R. Parthasarathy, The nature of halogen.cntdot.cntdot.cntdot.hAlOgen interactions: are short halogen contacts due to specific attractive forces or due to close packing of nonhalogen atoms? *J. Am. Chem. Soc.* 111 (1989) 8725–8726, <https://doi.org/10.1021/ja00205a027>.
- [41] P. Auffinger, F.A. Hays, E. Westhof, P.S. Ho, Halogen bonds in biological molecules, *Proc. Natl. Acad. Sci. U. S. A.* 101 (2004) 16789 LP–16794, <https://doi.org/10.1073/pnas.0407607101>.
- [42] F.C. Pigge, V.R. Vangala, D.C. Swenson, Relative importance of X…O=C vs. X…X halogen bonding as structural determinants in 4-halotriarylbenzenes, *Chem. Commun. (Camb.)* (2006) 2123–2125, <https://doi.org/10.1039/B603110B>.
- [43] M.J. Turner, J.J. McKinnon, S.K. Wolff, D.J. Grimwood, P.R. Spackman, D. Jayatilaka, M.A. Spackman, *Cryst. Expl.* 17 (2017).
- [44] S. Thakur, D.M. Gil, A. Frontera, S. Chattopadhyay, Exploration of Br…O halogen bonding interactions in dinuclear vanadium(V) complexes with Schiff base ligands, *Polyhedron* 187 (2020), 114676, <https://doi.org/10.1016/j.poly.2020.114676>.
- [45] S.K. Seth, D. Sarkar, T. Kar, Use of π - π forces to steer the assembly of chromone derivatives into hydrogen bonded supramolecular layers: crystal structures and Hirshfeld surface analyses, *CrystEngComm* 13 (2011) 4528–4535, <https://doi.org/10.1039/C1CE05037K>.
- [46] P.R. Grabowski, What is the covalency of hydrogen bonding? *Chem. Rev.* 111 (2011) 2597–2625, <https://doi.org/10.1021/cr800346f>.
- [47] U. Koch, P.L.A. Popelier, Characterization of C–H–O hydrogen bonds on the basis of the charge density, *J. Phys. Chem.* 99 (1995) 9747–9754, <https://doi.org/10.1021/j100024a016>.
- [48] E. Espinosa, I. Alkorta, J. Elguero, E. Molins, From weak to strong interactions: a comprehensive analysis of the topological and energetic properties of the electron density distribution involving X–H…F–Y systems, *J. Chem. Phys.* 117 (2002) 5529–5542, <https://doi.org/10.1063/1.1501133>.
- [49] P.R. Varadwaj, A. Varadwaj, B.-Y. Jin, Significant evidence of C…O and C…C long-range contacts in several heterodimeric complexes of CO with CH₃–X, should one refer to them as carbon and dicarbon bonds!, *Phys. Chem. Chem. Phys.* 16 (2014) 17238–17252, <https://doi.org/10.1039/C4CP01775G>.
- [50] N.D. Rajendran, N. Mookan, I. Samuel, S.B. Mookan, Experimental validation of bifurcated hydrogen bond of 2,5-lutidinium bromanilate and its charge density distribution, *Chem. Pap.* 74 (2020) 2689–2699, <https://doi.org/10.1007/s11696-020-01107-3>.
- [51] E.R. Johnson, S. Keinan, P. Mori-Sánchez, J. Contreras-García, A.J. Cohen, W. Yang, Revealing noncovalent interactions, *J. Am. Chem. Soc.* 132 (2010) 6498–6506, <https://doi.org/10.1021/ja100936w>.
- [52] C.C.D. CrysAlisPro, R.E.D. CrysAlisPro, including ABSPACK, 2009.
- [53] G. Sheldrick, Crystal structure refinement with SHELXL, *Acta Crystallogr. Sect. C* 71 (2015) 3–8, <https://doi.org/10.1107/S2053229614024218>.
- [54] G. Sheldrick, A short history of SHELX, *Acta Crystallogr. Sect. A* 64 (2008) 112–122.
- [55] M.J. Frisch, G.W. Trucks, H.B. Schlegel, G.E. Scuseria, M.A. Robb, J.R. Cheeseman, G. Scalmani, V. Barone, G.A. Petersson, H. Nakatsuji, X. Li, M. Caricato, A. V. Marenich, J. Bloino, B.G. Janesko, R. Gomperts, B. Mennucci, H.P. Hratchian, J. V. Ortiz, A.F. Izmaylov, J.L. Sonnenberg, F. Ding Williams, F. Lipparini, F. Egidi, J. Goings, B. Peng, A. Petrone, T. Henderson, D. Ranasinghe, V.G. Zakrzewski, J. Gao, N. Rega, G. Zheng, W. Liang, M. Hada, M. Ehara, K. Toyota, R. Fukuda, J. Hasegawa, M. Ishida, T. Nakajima, Y. Honda, O. Kitao, H. Nakai, T. Vreven, K. Throssell, J.A. Montgomery Jr., J.E. Peralta, F. Ogliaro, M.J. Bearpark, J. J. Heyd, E.N. Brothers, K.N. Kudin, V.N. Staroverov, T.A. Keith, R. Kobayashi, J. Normand, K. Raghavachari, A.P. Rendell, J.C. Burant, S.S. Iyengar, J. Tomasi, M. Cossi, J.M. Millam, M. Klene, C. Adamo, R. Cammi, J.W. Ochterski, R.L. Martin, K. Morokuma, O. Farkas, J.B. Foresman, D.J. Fox, *Gaussian 16 Rev. C.01*, 2016.
- [56] C.F. Mackenzie, P.R. Spackman, D. Jayatilaka, M.A. Spackman, *CrystalExplorer model energies and energy frameworks: extension to metal coordination compounds, organic salts, solvates and open-shell systems*, *IUCrJ.* 4 (2017) 575–587.